SABA Publishing

Journal of Mathematical Analysis and Modeling
jmam.sabapub.com
ISSN 2709-5924

J Math Anal & Model
(2025)6(3) : 84-112
doi:10.48185/jmam.v6i3.1843

TRANSMISSION DYNAMICS OF CHOLERA DISEASE USING FRACTIONAL–ORDER MODEL

VICTORY ONYEKACHI OBI [a], FRANKLINE CHIDI EZE [b,*]
KIZTO UGOCHUKWU NWAJERI [c]

[a] Department of Mathematics, Federal University of Technology, Owerri, Nigeria
[b] Department of Mathematics, Imo State University, Owerri, Nigeria
[c] Department of Mathematics, Federal University of Technology, Owerri, Nigeria

• *Received: 11 October 2025* • *Accepted: 03 November 2025* • *Published Online: 31 December 2025*

Abstract

Traditional epidemic models usually use integer-order derivatives, which often fail to capture inherent memory and hereditary effects involved in the transmission of diseases. This work presents a cholera model of fractional order that is formulated within the Atangana–Baleanu fractional derivative, which possesses a non-local and nonsingular kernel. The existence and uniqueness of the proposed model were analyzed utilizing Banach's and Krasnoselskii's fixed point theorems, while the stability analysis results indicated that the disease-free equilibrium of the model is locally asymptotically stable if the basic reproduction number is less than unity. Numerical simulations are presented using the predictor–corrector scheme in the Atangana–Baleanu framework, showing the significant impact of the fractional order on the system dynamics. Our results suggest that the memory-dependent transmission patterns exhibited by cholera are captured more exactly by the fractional-order formulation than its classical integer-order counterpart. Overall, this paper confirms the mathematical flexibility and improved realism of the Atangana–Baleanu fractional operator within the context of modeling cholera dynamics and further advances the theoretical developments underlying fractional epidemic modeling.

Keywords: Cholera, fractional order derivatives, simulations, convergence, reproduction number.

1. Introduction

Waterborne bacterial diseases remain a high public health burden in developing regions where access to safe water and adequate sanitation is limited. Among these, cholera caused by Vibrio cholerae remains significant, as evidenced by repeated outbreaks throughout Africa, Asia, and parts of Latin America. While effective prevention and control through improved sanitation, vaccination, and oral rehydration therapy have been established, cholera remains endemic in many countries. This has pointed to the need for

*Corresponding author: ezefrankline@imsuonline.edu.ng

increasingly sophisticated mathematical models capable of representing complex cholera transmission dynamics.

Cholera emerged as a significant global health concern in 1817 when the first pandemic originated in India, following the bacteria's spread from its initial reservoir in the Ganges Delta. According to the [46], there have since been six additional cholera pandemics. The second pandemic started in Russia in 1829 and expanded into Europe, reaching many major cities in Canada and the United States by 1834. The third pandemic, which began in India in 1852, was the deadliest, spreading to Europe, the United States, Mexico, and the West Indies, with the year 1854 recording over 23,000 fatalities in Great Britain. The fourth and fifth pandemics occurred in 1863 and 1881, respectively, though these outbreaks were less deadly and the disease further spread to China, Japan, and South America. The sixth pandemic lasted from 1899 to 1923 and significantly impacted India, the North African coast, and Arabia, with an estimated 34,000 deaths in Egypt over three months, and 4,000 Muslim pilgrims who died during Hajj in Mecca in 1902. After this period, cholera declined in many regions but remained endemic in the Indian subcontinent. The seventh pandemic, noted by [15], began in 1961 in Indonesia, spreading through Asia, the Middle East, and Africa. This pandemic saw a resurgence in Africa, where 90 percent of cholera cases reported to the WHO in 1990 were from that region. Although cholera incidence has decreased in developed nations, it persists in Africa. The most recent severe outbreak in Africa occurred in Zimbabwe from 2008 to 2009, resulting in 4,287 deaths amid an economic crisis. Additionally, Haiti experienced a severe cholera outbreak from 2010 to 2011 following a major earthquake, with contaminated water from the Artibonite River being a primary cause. By October of that year, the WHO reported 473,649 cholera cases and 6,631 deaths. Cholera remains endemic in many regions, particularly in Africa, China, and India [43], where access to safe drinking water and sanitation is often limited. In India and Bangladesh, seasonal cholera outbreaks correlate with changes in water temperature, monsoon cycles, El Niño rains, and zooplankton levels. Nigeria has also seen a rise in outbreaks since the first recent occurrence in 1970. Cholera is a waterborne illness contracted through the ingestion of contaminated water or food, leading to mild symptoms or none at all, with the bacterium being shed into the environment through feces and vomit [46]. The disease spreads via the fecal-oral route, with transmission occurring when feces contaminated with the bacteria contaminate water consumed by individuals.

Cholera is an acute infectious disease caused by a bacterium that can be transmitted through contact with infected individuals or contaminated environments. It is characterized by severe diarrhea and vomiting. The occurrence of cholera is generally linked to inadequate sanitation, poor food hygiene, and untreated water. The cholera bacterium produces a toxin that interferes with the body's ability to absorb fluids, leading to dehydration. If untreated, individuals may face severe dehydration and potentially death within two to three hours. Treatment depends on the level of dehydration, with oral rehydration solutions used for mild to moderate cases, while severe cases require aggressive intravenous rehydration. Public health measures that can help prevent and control cholera include improving food safety, ensuring access to safe drinking water, maintaining proper sanitation, and enhancing surveillance. Health education plays a crucial role in increasing public awareness of preventive measures. In some cases, the symptoms and dynamics of

the disease may be unclear. Additionally, estimating the reproductive numbers for cholera outbreaks, such as those in Zimbabwe in 2008/2009, can be complex. As a result, many researchers utilize mathematical models to study disease transmission. These models serve as effective tools for explaining complex systems, examining the impacts of various factors, and making informed predictions about future behavior. In recent years, researchers have focused on developing mathematical models that utilize fractional-order derivatives. Various studies, including those by [28, 17, 42, 2, 3, 4], [40], [21, 25],[7, 14], [9] and [26]. Furthermore, numerous real-life phenomena modeled through fractional derivatives demonstrate significant fractional dynamical behavior, including a fractional-order multi-vaccination model for COVID-19 [36] and fractional advection-dispersion models [30], [20] and [28],

Mathematical modeling has been one important means of studying infectious disease spread and control, providing important estimates of key parameters such as the basic reproduction number and efficacies of interventions. Traditional modeling of cholera infections, from the models proposed by [47, 34, 11, 5, 17], has efficiently described the dynamics of infection and, consequently, the impact of interventions such as vaccination, treatment, and sanitation. However, many of these models have been based on integer-order differential equations, which implicitly assume that the rate of change in each compartment depends upon the current state of the system. This assumption overlooks inherent biological memory and hereditary features related to latency, immune response, and even bacterial persistence in the environment. Because of this, integer-order models cannot capture the long-term temporal correlations characteristic of real cholera dynamics.

Recent advances in fractional calculus have introduced a powerful mathematical framework for modeling systems possessing memory and non-local interactions. Fractional-order derivatives generalize classical differentiation by taking into account the past states of the system, hence giving a more accurate and flexible approach to describing biological and epidemiological processes. Among them, the so-called Atangana–Baleanu fractional derivative, defined with a non-singular and non-local Mittag–Leffler kernel, has gained considerable attention owing to its properties: avoiding the singularities that affect other operators, such as Caputo or Riemann–Liouville, it maintains relevant physical properties. This operator has been effectively applied in the modeling of diseases like COVID-19 [36] and [33, 3, 1, 41, 12, 19, 22, 6, 36], but its potential remains mainly unexplored in capturing the memory-dependent transmission patterns of cholera.

This study fills this gap by developing and analyzing a fractional-order cholera transmission model based on the Atangana-Baleanu fractional derivative. The model comprises relevant epidemiological compartments and explicitly accounts for memory effects in the dynamics. We establish the existence and uniqueness of the solution for the model using Banach's and Krasnoselskii's fixed point theorems. The local stability of the disease-free equilibrium is obtained with respect to the basic reproduction number, which shows the analytical conditions for disease control. Finally, we carry out numerical simulations using a predictor-corrector method adapted to the AB framework to demonstrate how changes in the fractional order lead to changes in the temporal evolution of the system.

The novel contributions of this paper are:

1. We propose a new Atangana–Baleanu fractional-order cholera model that integrates memory effects into the transmission dynamics.

2. We provide a rigorous existence, uniqueness, and stability analysis using modern fixed point and fractional calculus theory.
3. We demonstrate through simulations that the fractional-order parameter significantly alters disease dynamics, offering a more realistic depiction of cholera progression compared to classical integer-order models.

Overall, this work extends the theory of fractional epidemic modeling and provides a mathematically grounded framework for understanding and controlling cholera transmission in environments where historical and memory effects play a critical role.

2. Model Formulation

In this paper, the total human population is divided into four classes of epidemiological compartments depending on their infection status: susceptible people, $S_h(t)$, who are at risk of contracting cholera due to contact with contaminated water or food; exposed people, $E_h(t)$, who have been infected but are not yet infectious because they are in the latent or incubation period of the disease; asymptomatically infected people, $I_h(t)$, who are infected and carry and shed the pathogen but do not show clinical symptoms of the disease; and recovered or removed individuals, $R_h(t)$, consisting of those who recovered from the infection and develop temporary immunity or those who are removed from the susceptible pool of the total population due to natural deaths or disease-induced mortality. In the model, besides the human population, an environmental compartment is used to represent the role of the pathogen in disease persistence and transmission. The environmental compartment is modeled by $B_v(t)$, representing the concentration of Vibrio cholera present in the aquatic environment, for example, rivers, ponds, or contaminated water sources. This compartment is indispensable in light of the prevailing principle that the main mode of transmission of cholera involves the ingestion of water or food containing the bacteria. The concentration of $B_v(t)$ grows as infectious individuals shed the pathogen into the environment in the form of feces and vomit, and decreases over time due to natural bacterial decay and water purification processes. The model incorporates five dynamic components: $S_h(t)$, $E_h(t)$, $I_h(t)$, $R_h(t)$, and $B_v(t)$, all of which describe both human-to-environment and environment-to-human cholera transmission pathways. The resulting framework provides a realistic basis for analyzing disease dynamics, estimating threshold parameters such as the basic reproduction number, and investigating the impact of fractional-order dynamics on the persistence and control of cholera in a given population.
The fractional dynamic model describing the temporal evolution of the sizes of the compartments is based on the following assumptions:

- The population of the susceptible class will keep increasing if there is no contact with the infectious class. Also, the population of the susceptible class will decrease at a rate proportional to its current population if there is a contact with the infectious class.

- The rate at which the susceptible becomes infected is proportional to the number of encounters between susceptible and infected individuals. This in turn is proportional to the product of the two population.

- The rate of transition from class I_h to class R_h is proportional to I_h. This means that the number of individuals moving from the infectious class I_h to the recovered or removed class R_h depends directly on the current number of infectious individuals in the population.
- We also assume the population is completely homogeneous and there are deaths caused by the cholera disease.

The total population with time is denoted as $N_h(t) = S_h(t) + E_h(t) + I_h(t) + R_h(t)$. The parameter νh denotes the rate of constant recruitment to the human population, μh denotes the natural mortality rate. The quantities $\frac{\Theta h S_h I_h}{N_h}$ and $\psi h S_h B_v$ denote the rate at which S_h is exposed to cholera and contaminated water and moved to E_h compartment from where they are moved to I_h based on the latent period. The parameter $\Theta h \alpha$ denotes the contact rate of human to human, ϖ represents the mortality rate induced by the disease. The remaining parameters are properly defined in Table 3.

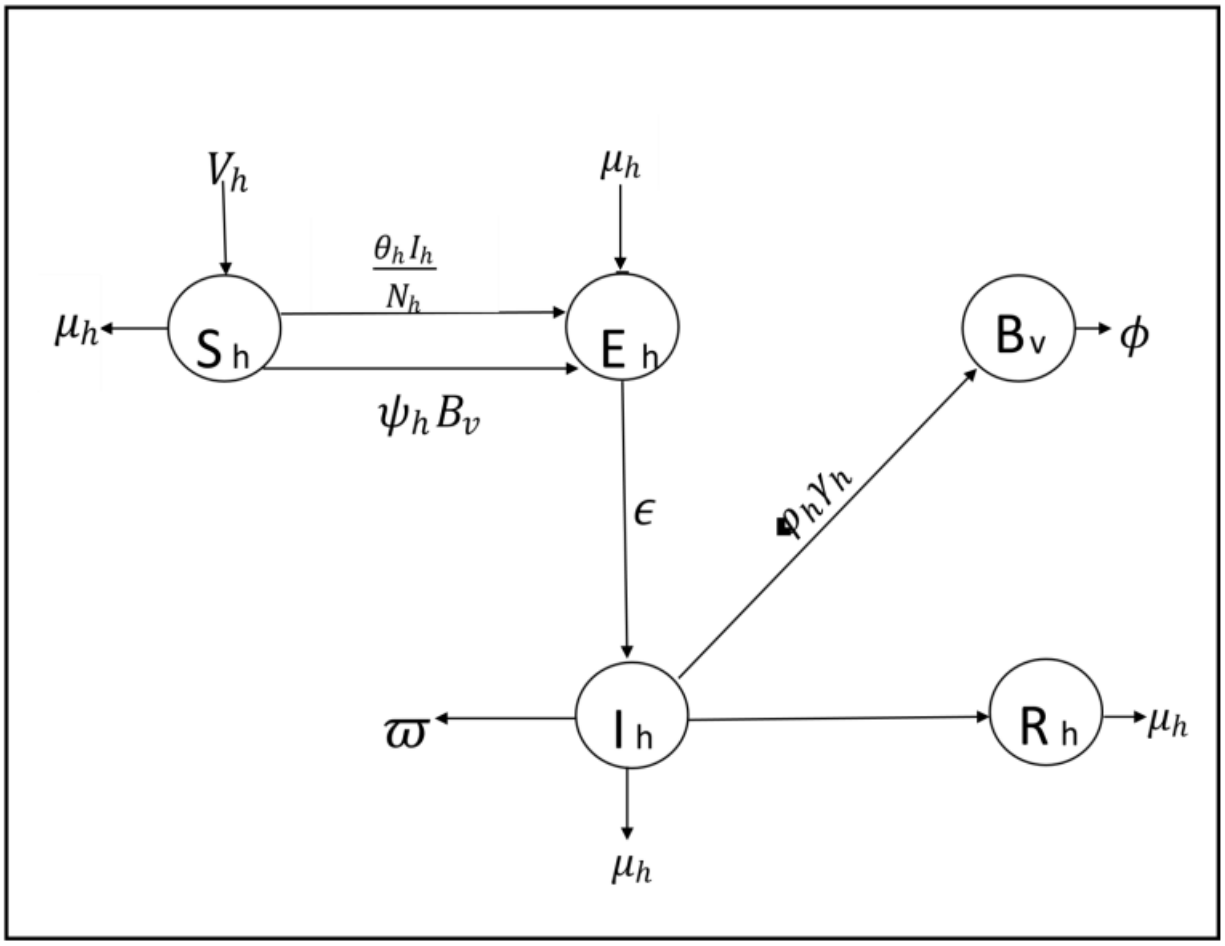

Figure 1: Schematic Diagram of Cholera

Table 1: Description of parameters in the model (2.1).

Parameter	Interpretation
Υ_h	Human shedding vibrose bacteria
ϕ	Half satuation Concentration vibrio cholerae
ν_h	Recruitment rate
μ_h	Natural death rate
φ_h	Removal rate
ϖ	Motality rate caused by the disease
ψ_h	Higher rate of virus transmission
Θ_h	Rate of contact
ε	Progression rate

Recently, several researchers and scientists have noted the growing importance of fractional calculus. This area has been recognized as particularly useful for describing processes and phenomena that exhibit memory effects. Fractional order mathematical systems have been extensively examined in relation to various real-world issues across fields such as science, biology, chemistry, and engineering. Derivatives of fractional order have been found to offer a more comprehensive understanding of the dynamics of various infectious diseases compared to classical calculus, due to the non-local characteristics of fractional order operators, in contrast to the local characteristics of classical calculus. Given these advantages, we present the Atangana-Baleanu fractional-order system of cholera disease as follows. The model equation is given by:

$$\begin{aligned}
{}_0^{\mathcal{ABC}}\mathcal{D}_t^p S_h(t) &= \nu h - \frac{\Theta h S_h I_h}{N_h} - \mu h S_h - \psi h B_v S_h,\\
{}_0^{\mathcal{ABC}}\mathcal{D}_t^p E_h(t) &= \frac{\Theta h S_h I_h}{N_h} + \psi h S_h B_v - (\mu h + \epsilon) E_h,\\
{}_0^{\mathcal{ABC}}\mathcal{D}_t^p I_h(t)(t) &= \epsilon E_h - (\varphi h + \varpi + \mu h) I_h,\\
{}_0^{\mathcal{ABC}}\mathcal{D}_t^p B_v(t) &= \varphi h \Upsilon h I_h - \phi B_v,\\
{}_0^{\mathcal{ABC}}\mathcal{D}_t^p R_h(t)(t) &= \varphi h I_h - \mu h R_h,
\end{aligned} \tag{2.1}$$

with the corresponding initial condition

$$\begin{aligned}
S_h(0) = S_{h(0)} \geqslant 0, \quad E_h(0) = E_{h(0)} \geqslant 0, \quad , I_h(0) = I_{h(0)} \geqslant 0,\\
B_v(0) = B_{v(0)} \geqslant 0, \quad R_h(0) = R_{h(0)} \geqslant 0.
\end{aligned} \tag{2.2}$$

3. Results and Analysis of the model

In this chapter, we present the analysis and the solution of the Atangana–Baleanu fractional cholera model (2.1)–(2.2) which includes investigation of the disease–free equlibrium state, basic reproduction number, existence and uniqueness of the system solution using fixed point theorem. In another note, the numerical algorithm for the solution of the fractional system including its numerical simulations and discussions are also presented.Also matlab Software is used to obtain the numerical simulation figures

3.1. Qualitative analysis of the fractional model

This analysis focuses on the fractional model concerning the existence of a disease-free equilibrium state $\mathbb{E}^0$, the basic reproduction number $\mathcal{R}_0$, which represents the anticipated number of secondary cases produced by a single typical index case in a wholly susceptible population, local asymptotic stability, as well as the existence and uniqueness of the model.

3.2. Disease-free equilibrium state

Disease-free equilibrium state, $\mathbb{E}^0$ simply means the point where there is total absence of cholera within the population,that is where compartment $E_h = I_h = B_v = 0$. Thus by setting $E_h = I_h = B_v = 0$ into (2.1) and equating each system to zero, we obtain the disease–equilibrium state.
At DFE, all the Disease Classes equal to Zero. That is, $E_h = I_h = B_v = R_h = 0$. Thus, the model reduces to

$$\nu_H - \mu_h S_h = 0.$$

Hence,

$$S_h = \frac{\nu_H}{\mu_h}.$$

This therefore implies that,

$$\mathbb{E}^0 = \left(S_h^0, E_h^0, I_h^0, B_v^0, R_h^0\right) = \left(\frac{\nu h}{\mu h}, 0, 0, 0, 0\right).$$

3.3. Basic reproduction number, $\mathcal{R}0$

Using the next generation matrix or the spectral radius method obtained from Driessche and Watmough 2002 [Driessche and Watmough (2002)], the basic reproduction number $\mathcal{R}0 = \rho(FV^{-1})$, which is known as the spectral radius, is the largest eigenvalues of the matrix $|FV^{-1}|$. Here matrix F is the rate of new infections in different compartment differentiated with respect to I_h and B_v and evaluated at $\mathbb{E}^0$ which is the disease–free equilibrium. Matrix V defines the rate of transfer of infectives from one compartment to another.

Let $X = \left(I_h, B_v, S_h\right)^T$ so that system (2.1) can be written as

$$\frac{dX}{dt} = F(X) - V(X),$$

where

$$F(X) = \begin{pmatrix} \frac{\Theta h S_h I_h}{N_h} + \psi h S_h B_v \\ 0 \\ 0 \end{pmatrix}, \quad V(X) = \begin{pmatrix} (\mu h + \varepsilon) E_h \\ (\varphi h + \varpi + \mu h) I_h \\ \phi B_v - \varphi h \Upsilon h I_h \end{pmatrix}.$$

Thus, the Jacobian matrices $F(X)$ and $V(X)$ evaluated at the disease–free equilibrium $\mathbb{E}^0$ are respectively,

$$= \frac{\partial F}{\partial t}(\mathbb{E}^0) \begin{pmatrix} F & 0 & 0 \\ 0 & 0 & 0 \\ 0 & 0 & 0 \end{pmatrix}, \quad \frac{\partial V}{\partial t}(\mathbb{E}^0) = \begin{pmatrix} V & 0 & 0 \\ 0 & 0 & 0 \\ J_1 & J_2 & J_3 \end{pmatrix},$$

where

$$F = \begin{pmatrix} 0 & \Theta h a & \frac{\psi h \nu h}{\mu h} \\ 0 & 0 & 0 \\ 0 & 0 & 0 \end{pmatrix}, \quad V = \begin{pmatrix} \mu h + \epsilon & 0 & 0 \\ -\epsilon & \varphi h + \varpi + \mu h & 0 \\ 0 & -\varphi h \Upsilon h & \phi \end{pmatrix}.$$

Then

$$V^{-1} = \begin{pmatrix} \frac{1}{\mu h + \epsilon} & 0 & 0 \\ \frac{\epsilon}{(\mu h+\epsilon)(\varphi h+\varpi+\mu h)} & \frac{1}{\varphi h+\varpi+\mu h} & 0 \\ \frac{\varphi h \epsilon \Upsilon h}{\phi(\mu h+\epsilon)(\varphi h+\varpi+\mu h)} & \frac{\varphi h \Upsilon h}{\phi(\varphi h+\varpi+\mu h)} & \frac{1}{\phi} \end{pmatrix},$$

$$FV^{-1} = \begin{pmatrix} \frac{\epsilon(\phi\Theta h+\psi h\nu h\Upsilon h\varphi h)}{\phi(\mu h+\epsilon)(\varphi h+\varpi+\mu h)} & \frac{\Theta h\phi\mu h+\psi h\nu h\varphi h\Upsilon h}{\phi\mu h(\varphi h+\varpi+\mu h)} & \frac{\psi h\nu h}{\mu h\phi} \\ 0 & 0 & 0 \\ 0 & 0 & 0 \end{pmatrix}$$

It follows that

$$\left|FV^{-1} - \lambda I_3\right| = \begin{vmatrix} \frac{\epsilon(\phi\Theta h a+\psi h\nu h\Upsilon h\varphi h)}{\phi(\mu h+\epsilon)(\varphi h+\varpi+\mu h)} - \lambda & \frac{\Theta h a\phi\mu h+\psi h\nu h\varphi h\Upsilon h}{\phi\mu h(\varphi h+\varpi+\mu h)} & \frac{\psi h\nu h}{\mu h\phi} \\ 0 & -\lambda & 0 \\ 0 & 0 & -\lambda \end{vmatrix} = 0,$$

from which we obtain $\lambda_1 = \lambda_2 = 0$ and $\lambda_3 = \frac{\epsilon(\phi\Theta h a+\psi h\nu h\Upsilon h\varphi h)}{\phi(\mu h+\epsilon)(\varphi h+\varpi+\mu h)}$. Since the largest eigenvalue is λ_3 and due to the positive nature of the parameters, then the basic reproduction number of the fractional system (2.1) is

$$\mathcal{R}0 = \frac{\epsilon(\phi\Theta h a + \psi h\nu h\Upsilon h\varphi h)}{\phi(\mu h + \epsilon)(\varphi h + \varpi + \mu h)}. \tag{3.1}$$

Theorem 3.1. *The disease-free equilibrium $\mathbb{E}^0$ is locally assymptotically stable if $\mathcal{R}0 < 1$ and unstable if $\mathcal{R}0 > 1$.*

Proof. The Jacobian matrix $\mathcal{J}$ evaluated at the disease-free eqilibrium state, $\mathbb{E}^0$ is given by partially differentiating the indepedent variables in (2.1) with respect to S_h, E_h, I_h, B_v and R_h is

$$\mathcal{J}(\mathbb{E}^0) = \begin{bmatrix} -\mu h & 0 & -\frac{\Theta h a\nu h}{\mu h} & 0 & -\frac{\psi h\nu h}{\mu h} \\ 0 & -(\mu h+\epsilon) & \frac{\Theta h a\nu h}{\mu h} & 0 & \frac{\psi h\nu h}{\mu h} \\ 0 & \epsilon & -(\varphi h+\varpi+\mu h) & 0 & 0 \\ 0 & 0 & \varphi h & -\mu h & 0 \\ 0 & 0 & \varphi h\Upsilon h & 0 & -\phi \end{bmatrix}.$$

It then leads to the following determinant of the square matrix,

$$\left|\mathcal{J}(\mathbb{E}^0)-\lambda I_5\right| = \begin{vmatrix} -\mu h-\lambda & 0 & -\frac{\Theta h a \nu h}{\mu h} & 0 & -\frac{\psi h \nu h}{\mu h} \\ 0 & -(\mu h+\epsilon)-\lambda & \frac{\Theta h a \nu h}{\mu h} & 0 & \frac{\psi h \nu h}{\mu h} \\ 0 & \epsilon & -(\varphi h+\varpi+\mu h)-\lambda & 0 & 0 \\ 0 & 0 & \varphi h & -\mu h-\lambda & 0 \\ 0 & 0 & \varphi h \Upsilon h & 0 & -\phi-\lambda \end{vmatrix} = 0,$$

which has the following characteristic equation,

$$(\lambda+\mu h)^2\left((\lambda+\phi)\left((\mu h+\epsilon+\lambda)(\varphi h+\varpi+\mu h+\lambda)-\frac{\Theta h a \nu h \epsilon}{\mu h}\right)-\frac{\psi h \nu h \epsilon \varphi h \Upsilon h}{\mu h}\right) = 0.$$

So $\lambda=-\mu h$ with algebraic multiplicity of 2 are two of the eigenvalues of the Jacobian matrix $\mathcal{J}(\mathbb{E}^0)$ which satisfies the negativity requirements for stability since $\mu h>0$. The rest of eigenvalues can be obtained using

$$\lambda^3+\alpha_1\lambda^2+\alpha_2\lambda+\alpha_3 = 0,$$

where

$$\begin{aligned} \alpha_1 &= 2\mu h+\epsilon+\varphi h+\varpi+\phi, \\ \alpha_2 &= \frac{\phi\epsilon\Theta h a(\mu h-\nu h\mathcal{R}0)+\mu h(\epsilon\psi h\nu h\Upsilon h\varphi h+\phi^2\mathcal{R}0(2\mu h+\varphi h+\varpi+\epsilon))}{\mu h\phi\mathcal{R}0}, \\ \alpha_3 &= \frac{\epsilon\Theta h a(\phi\mu h-\nu h\mathcal{R}0)+\mu h\nu h\epsilon\psi h\Upsilon h\varphi h\left(1-\frac{\mathcal{R}0}{\mu h}\right)}{\mu h\mathcal{R}0}. \end{aligned}$$

. Adopting similar argument from (Khan and Atagana,(2020)), we see that $\alpha_3>0$ when $\mathcal{R}0<1$. So by Routh-Herwitz system which is used to determine whether all roots of a polynomials have negative real parts, graphicx

$$\begin{aligned} \alpha_1\alpha_2-\alpha_3 = (2\mu h+\epsilon+\varphi h+\varpi+\phi)&\left(\frac{\phi\epsilon\Theta h a(\mu h-\nu h\mathcal{R}0)+\mu h(\epsilon\psi h\nu h\Upsilon h\varphi h+\phi^2\mathcal{R}0(2\mu h+\varphi h+\varpi+\epsilon))}{\mu h\phi\mathcal{R}0}\right) \\ &-\left(\frac{\epsilon\Theta h a(\phi\mu h-\nu h\mathcal{R}0)+\mu h\nu h\epsilon\psi h\Upsilon h\varphi h\left(1-\frac{\mathcal{R}0}{\mu h}\right)}{\mu h\mathcal{R}0}\right)>0 \end{aligned} \tag{3.2}$$

By the same criteria of Routh-Herwitz, the eigenvalues of $J(\mathbb{E}^0)$ are all negatives when $\mathcal{R}0<1$. Therefore if $\mathcal{R}0<1$, system (2.1)–(2.2) evaluated at the disease-free equilibrium $\mathbb{E}^0$ is locally asymptotically stable. □

The $\mathcal{R}0 < 1$ means that each person who gets the cholera disease will infect less than one person before recovering or dying while the $\mathcal{R}0 > 1$ means that each person who gets the cholera disease will infect more than one person, therefore, the epidemic will spread into the population.

3.4. Existence and Uniqueness of Solution

We examine the existence and uniqueness of the solution to the model (2.1)–(2.2) using a fixed point theorem. The existence and uniqueness of solutions is a crucial aspect of differential equations. The study of differential equations that involve fractional order derivatives and integrals has been explored by various researchers [26, 6, 7, 36]. In this work, we will adopt a similar approach to those in the referenced studies. To investigate the existence and uniqueness of the solution for our model, we will reformulate our fractional order model as follows:

$$\begin{aligned}
{}_0^{\mathcal{ABC}}\mathcal{D}_t^p S_h(t) &= \mathcal{F}_1\left(t, S_h, E_h, I_h, B_v, R_h\right),\\
{}_0^{\mathcal{ABC}}\mathcal{D}_t^p E_h(t) &= \mathcal{F}_2\left(t, S_h, E_h, I_h, B_v, R_h\right),\\
{}_0^{\mathcal{ABC}}\mathcal{D}_t^p I_h(t) &= \mathcal{F}_3\left(t, S_h, E_h, I_h, B_v, R_h\right),\\
{}_0^{\mathcal{ABC}}\mathcal{D}_t^p B_v(t) &= \mathcal{F}_4\left(t, S_h, E_h, I_h, B_v, R_h\right),\\
{}_0^{\mathcal{ABC}}\mathcal{D}_t^p R_h(t) &= \mathcal{F}_5\left(t, S_h, E_h, I_h, B_v, R_h\right),
\end{aligned} \tag{3.3}$$

where $\mathcal{F}_n = \mathcal{F}_n\left(t, S_h, E_h, I_h, B_v, R_h\right)$ for $n = 1,2,3,4,5$ is given by

$$\begin{cases}
\mathcal{F}_1 = \nu h - \frac{\Theta h S_h I_h}{N_h} - \mu h S_h - \psi h B_v S_h,\\
\mathcal{F}_2 = \frac{\Theta h S_h I_h}{N_h} + \psi h S_h B_v - (\mu h + \epsilon) E_h,\\
\mathcal{F}_3 = \epsilon E_h - (\varphi h + \varpi + \mu h) I_h,\\
\mathcal{F}_4 = \varphi h \Upsilon h I_h - \phi B_v,\\
\mathcal{F}_5 = \varphi h I_h - \mu h R_h.
\end{cases} \tag{3.4}$$

Using the above illustration, the Atangana–Baleanu fractional model (2.1) can be written as

$$\begin{cases}
{}_0^{\mathcal{ABC}}\mathcal{D}_t^p y(t) = \mathcal{G}(t, y(t)), \qquad p \in (0,1], \qquad t \in [0,T],\\
y(0) = y_0 \in \mathbb{R}^+,
\end{cases} \tag{3.5}$$

where $\mathcal{G} : [0,T] \times \mathbb{R} \to \mathbb{R}$ is continuous and

$$\begin{cases}
y(t) = \left(S_h, E_h, I_h, B_v, R_h\right)^T,\\
y_0 = \left(S_{h0}, E_{h0}, I_{h0}, B_{v0}, R_{h0}\right)^T,\\
\mathcal{G}(t, y(t)) = \mathcal{F}_n\left(t, S_h, E_h, I_h, B_v, R_h\right)^T, \quad \text{where } n = 1,2,3,4,5.
\end{cases} \tag{3.6}$$

where $(.)^T$ denotes the transpose of the vector. Using Lemma (**??**) The initial value problem (3.5) is equivalent to the following fractional order Volterra integral equation

$$y(t) = y_0 + \frac{1-p}{\mathcal{ABC}(p)}\mathcal{G}(t, y(t)) + \frac{p}{\mathcal{ABC}(p)\Gamma(p)}\int_0^t (t-s)^{p-1}\mathcal{G}(s, y(s))ds. \tag{3.7}$$

Next, we define the Banach space $\mathcal{U} = \bar{\mathcal{W}} \subset C[0,T]$ endowed with the supremum norm

$$\begin{aligned} \|y\|_\infty &= \sup_{t\in[0,T]} \{|y(t)|\}, \qquad y \in \mathcal{U}, \\ &= \sup_{t\in[0,T]} \{|S_h(t)| + |E_h(t)| + |I_h(t)| + |B_v(t)| + |R_h(t)|\}. \end{aligned}$$

For the purpose of subsequent analyses, we state the following proposition:

Proposition 3.2. *There exists constants* $m_0, m_1 > 0$ *such that*

$$\sup_{t\in[0,T]} |\mathcal{G}(t, y(t))| \leqslant m_0 + m_1 |y(t)|,$$

where $m_0, m_1 \in \mathbb{R}$.

In another note there exists a real number $\mathcal{L}c > 0$ *such that for any two solutions* $y1, y2 \in \mathcal{U}$, *then*

$$|\mathcal{G}(t, y1(t)) - \mathcal{G}(t, y2(t))| \leqslant \mathcal{L}c\, |y1(t) - y2(t)|,$$

where $\mathcal{L}c$ *is known as the Lipschitz constant.*

Furthermore, we introduce the set

$$\mathcal{B} = \{y \in \mathcal{U} : \|y\|_\infty \leqslant \beta eu\},$$

which is a closed subset of the Banach space of all continuous functions on $[0,T]$. From (**??**), we define the following operators;

$$\begin{cases} \mathcal{J}(y)(t) = y_0 + \frac{1-p}{\mathcal{ABC}(p)} \mathcal{G}(t, y(t)), \\ \mathcal{H}(y)(t) = \frac{p}{\mathcal{ABC}(p)\Gamma(p)} \int_0^t (t-s)^{p-1} \mathcal{G}(s, y(s)) ds. \end{cases} \tag{3.8}$$

Using theorem (**??**), we show that $\mathcal{H} = \mathcal{H}(y)(t)$ is compact and continuous (totally continuous). To achieve this, we show that the operator $\mathcal{H}$ is bounded and equi-continuous. Thus for any $w \in \bar{\mathcal{W}}$, $t \in [0,T]$ and using Proposition 3.2 we obtain

$$\begin{aligned} \|\mathcal{H}(y)\|_\infty &\leqslant \sup_{t\in[0,T]} \left| \frac{p}{\mathcal{ABC}(p)\Gamma(p)} \int_0^t (t-s)^{p-1} \mathcal{G}(s, y(s)) ds \right|, \\ &\leqslant \frac{p}{\mathcal{ABC}(p)\Gamma(p)} \int_0^t (t-s)^{p-1} \sup_{t\in[0,T]} |\mathcal{G}(s, y(s))|\, ds, \\ &\leqslant \frac{T^p}{\mathcal{ABC}(p)\Gamma(p)} \left(m_0 + m_1 \|y(t)\|_\infty\right). \end{aligned} \tag{3.9}$$

Thus from (3.9), we have that

$$\|\mathcal{H}(y)\|_\infty \leqslant \frac{T^p}{\mathcal{ABC}(p)\Gamma(p)} \left(m_0 + m_1 \|y(t)\|_\infty\right),$$

which shows that $\mathcal{H}$ is bounded.

In another note, for equi-continuity, suppose that $t_2 > t_1$ such that $t \in [0, T]$, we have

$$\begin{aligned}
|\mathcal{H}(y)(t_2) - \mathcal{H}(y)(t_1)| &= \left| \frac{p}{\mathcal{ABC}(p)\Gamma(p)} \left(\int_0^{t_2} (t_2 - s)^{p-1} \mathcal{G}(s, y(s)) ds - \int_0^{t_1} (t_1 - s)^{p-1} \mathcal{G}(s, y(s)) ds \right) \right| \\
&\leqslant \frac{p}{\mathcal{ABC}(p)\Gamma(p)} \left(\int_0^{t_1} \left((t_1 - s)^{p-1} - (t_2 - s)^{p-1} \right) |\mathcal{G}(s, y(s))| \, ds \right. \\
&+ \left. \int_{t_1}^{t_2} (t_2 - s)^{p-1} |\mathcal{G}(s, y(s))| \, ds \right), \\
&\leqslant \frac{(m_0 + m_1 \|y(t)\|_\infty)}{\mathcal{ABC}(p)\Gamma(p)} \left(2(t_2 - t_1)^p + t_1^p - t_2^p \right) \\
, \quad &\leqslant \frac{(m_0 + m_1 \beta e u)}{\mathcal{ABC}(p)\Gamma(p)} \left(2(t_2 - t_1)^p + t_1^p - t_2^p \right). \qquad (3.10
\end{aligned}$$

Clearly, the right hand side of (3.10), $|\mathcal{H}(y)(t_2) - \mathcal{H}(y)(t_1)| \to 0$ as $t_2 \to t_1$. Thus by well-known Arzela-Ascoli theorem, the operator $\mathcal{H}(y)(t)$ is uniformly continuous and relatively compact. Therefore, we can say that the operator $\mathcal{H}$ is totally continuous.

Moreso, we show that $\mathcal{J} = \mathcal{J}(y)(t)$ is a contraction based on Theorem (**??**) with the aid of Proposition 3.2. Thus

$$\begin{aligned}
\|\mathcal{J}(y1)(t) - \mathcal{J}(y2)(t)\| &= \left| y_0 + \frac{1-p}{\mathcal{ABC}(p)} \mathcal{G}(t, y1(t)) - \left(y_0 + \frac{1-p}{\mathcal{ABC}(p)} \mathcal{G}(t, y2(t)) \right) \right|, \\
&\leqslant \frac{1-p}{\mathcal{ABC}(p)} \sup_{t \in [0,T]} \|\mathcal{G}(t, y1(t)) - \mathcal{G}(t, y2(t))\|, \\
&\leqslant \frac{1-p}{\mathcal{ABC}(p)} \mathcal{L}c \|y1(t) - y2(t)\|. \qquad (3.11)
\end{aligned}$$

Thus from (3.11), we have that

$$\|\mathcal{J}(y1)(t) - \mathcal{J}(y2)(t)\|_\infty \leqslant \frac{1-p}{\mathcal{ABC}(p)} \mathcal{L}c \|y(t) - y2(t)\|_\infty,$$

which proves that the operator $\mathcal{J} = \mathcal{J}(y1)(t)$ is a contraction. Therefore $\mathcal{J}y + \mathcal{H}y = \mathcal{X}y$ has one fixed point and hence the fractional order system (2.1)–(2.2) has at least one solution.

Next, for the purpose of **uniqueness** of the solution, we consider the following theorem.

Theorem 3.3. *Using Proposition 3.2 and if the operator $\mathcal{X} = \mathcal{X}(y)$ is a contraction, then $\mathcal{X}$ has a unique fixed point such that the fractional order system (2.1)–(2.2) has a unique solution if and only if*

$$\left(\frac{1-p}{\mathcal{ABC}(p)} + \frac{T^p}{\mathcal{ABC}(p)\Gamma(p)} \right) \mathcal{L}c < 1. \qquad (3.12)$$

Proof. By Banach fixed point theorem, let $\mathcal{X} : \mathcal{U} \to \mathcal{U}$ be an operator defined as

$$\mathcal{X}(y) = y_0 + \frac{1-p}{\mathcal{ABC}(p)} \mathcal{G}(t, y(t)) + \frac{p}{\mathcal{ABC}(p)\Gamma(p)} \int_0^t (t - s)^{p-1} \mathcal{G}(s, y(s)) ds.$$

Thus for the solutions $y_1, y2 \in \mathcal{U}$ and $t \in [0, T]$, we obtain

$$\begin{aligned}
\|\mathcal{X}(y_1) - \mathcal{X}(y2)\|_\infty &\leqslant \sup_{t\in[0,T]} \left| y_0 + \frac{1-p}{\mathcal{ABC}(p)} \mathcal{G}(t, y1(t)) + \frac{p}{\mathcal{ABC}(p)\Gamma(p)} \int_0^t (t-s)^{p-1} \mathcal{G}(s, y1(s)) ds \right. \\
&- \left. \left(y_0 + \frac{1-p}{\mathcal{ABC}(p)} \mathcal{G}(t, y2(t)) + \frac{p}{\mathcal{ABC}(p)\Gamma(p)} \int_0^t (t-s)^{p-1} \mathcal{G}(s, y2(s)) ds \right) \right|, \\
&\leqslant \frac{1-p}{\mathcal{ABC}(p)} \sup_{t\in[0,T]} \|\mathcal{G}(t, y1(t)) - \mathcal{G}(t, y2(t))\| + \frac{p}{\mathcal{ABC}(p)\Gamma(p)} \int_0^t (t-s)^{p-1} \\
&\times \sup_{t\in[0,T]} \|\mathcal{G}(s, y1(s)) - \mathcal{G}(s, y2(s))\| \, ds, \\
&\leqslant \left(\frac{1-p}{\mathcal{ABC}(p)} + \frac{T^p}{\mathcal{ABC}(p)\Gamma(p)} \right) \mathcal{L}c \, \|y1(t) - y2(t)\|_\infty . \qquad (3.13)
\end{aligned}$$

Thus from (3.13), we have that

$$\|\mathcal{X}(y1) - \mathcal{X}(y2)\|_\infty \leqslant \left(\frac{1-p}{\mathcal{ABC}(p)} + \frac{T^p}{\mathcal{ABC}(p)\Gamma(p)} \right) \mathcal{L}c \, \|y1(t) - y2(t)\|_\infty ,$$

which proves that the operator $\mathcal{X}$ is a contraction and therefore by Banach's contraction principle, it possesses a unique fixed point. Hence the fractional order system (2.1)–(2.2) possesses a unique solution. □

3.5. Numerical scheme

In this section, we apply a numerical scheme proposed by Toufik and Atangana [Toufik and Atangana (2017)] to the formulated fractional order transmission of cholera disease system to obtain the numerical solution. This numerical scheme has a tremendous convergence property when applied. Using the initial condition (2.2) and the Atangana–Baleanu integral (**??**), we obtain the following Atangana–Baleanu fractional Volterra equation of the system (2.1) as;

$$\begin{aligned}
S_h(t) - S_h(0) &= \frac{(1-p)}{\mathcal{ABC}(p)} \mathcal{F}_1(t, S_h(t)) + \frac{p}{\mathcal{ABC}(p)\Gamma(p)} \int_0^t (t-s)^{p-1} \mathcal{F}_1(s, S_h(s)) \, ds, \\
E_h(t) - E_h(0) &= \frac{(1-p)}{\mathcal{ABC}(p)} \mathcal{F}_2(t, E_h(t)) + \frac{p}{\mathcal{ABC}(p)\Gamma(p)} \int_0^t (t-s)^{p-1} \mathcal{F}_2(s, E_h(s)) \, ds, \\
I_h(t) - I_h(0) &= \frac{(1-p)}{\mathcal{ABC}(p)} \mathcal{F}_3(t, I_h(t)) + \frac{p}{\mathcal{ABC}(p)\Gamma(p)} \int_0^t (t-s)^{p-1} \mathcal{F}_3(s, I_h(s)) \, ds, \\
B_v(t) - B_v(0) &= \frac{(1-p)}{\mathcal{ABC}(p)} \mathcal{F}_4(t, B_v(t)) + \frac{p}{\mathcal{ABC}(p)\Gamma(p)} \int_0^t (t-s)^{p-1} \mathcal{F}_4(s, B_v(s)) \, ds, \\
R_h(t) - R_h(0) &= \frac{(1-p)}{\mathcal{ABC}(p)} \mathcal{F}_5(t, R_h(t)) + \frac{p}{\mathcal{ABC}(p)\Gamma(p)} \int_0^t (t-s)^{p-1} \mathcal{F}_5(s, R_h(s)) \, ds.
\end{aligned} \qquad (3.14)$$

Now setting $t = t_{m+1}$ for $m = 0, 1, 2, \ldots$ into the above equation (3.14) we get

$$
\begin{aligned}
S_h(t_{m+1}) - S_h(0) &= \frac{(1-p)}{\mathcal{ABC}(p)}\mathcal{F}_1\left(t_m, S_h(t_m)\right) + \frac{p}{\mathcal{ABC}(p)\Gamma(p)}\sum_{k=0}^{m}\int_0^{t_{k+1}}(t_{m+1}-s)^{p-1}\mathcal{F}_1\left(s, S_h(s)\right)ds,\\
E_h(t_{m+1}) - E_h(0) &= \frac{(1-p)}{\mathcal{ABC}(p)}\mathcal{F}_2\left(t_m, E_h(t_m)\right) + \frac{p}{\mathcal{ABC}(p)\Gamma(p)}\sum_{k=0}^{m}\int_0^{t_{k+1}}(t_{m+1}-s)^{p-1}\mathcal{F}_2\left(s, E_h(s)\right)ds,\\
I_h(t_{m+1}) - I_h(0) &= \frac{(1-p)}{\mathcal{ABC}(p)}\mathcal{F}_3\left(t_m, I_h(t_m)\right) + \frac{p}{\mathcal{ABC}(p)\Gamma(p)}\sum_{k=0}^{m}\int_0^{t_{k+1}}(t_{m+1}-s)^{p-1}\mathcal{F}_3\left(s, I_h(s)\right)ds,\\
B_v(t_{m+1}) - B_v(0) &= \frac{(1-p)}{\mathcal{ABC}(p)}\mathcal{F}_4\left(t_m, B_v(t_m)\right) + \frac{p}{\mathcal{ABC}(p)\Gamma(p)}\sum_{k=0}^{m}\int_0^{t_{k+1}}(t_{m+1}-s)^{p-1}\mathcal{F}_4\left(s, B_v(s)\right)ds,\\
R_h(t_{m+1}) - R_h(0) &= \frac{(1-p)}{\mathcal{ABC}(p)}\mathcal{F}_5\left(t_m, R_h(t_m)\right) + \frac{p}{\mathcal{ABC}(p)\Gamma(p)}\sum_{k=0}^{m}\int_0^{t_{k+1}}(t_{m+1}-s)^{p-1}\mathcal{F}_5\left(s, R_h(s)\right)ds.
\end{aligned}
\tag{3.15}
$$

Using two–point Lagrange interpolation polynomial, we approximate $\mathcal{F}_1\left(s, S_h(s)\right)$, $\mathcal{F}_2\left(s, E_h(s)\right)$, $\mathcal{F}_3\left(s, I_h(s)\right)$, $\mathcal{F}_4\left(s, B_v(s)\right)$, $\mathcal{F}_5\left(s, R_h(s)\right)$, in (3.15) on the closed interval $[t_k, t_{k+1}]$ and obtain

$$
\begin{aligned}
\mathcal{F}_1\left(s, S_h(s)\right) &\approx \frac{\mathcal{F}_1\left(t_k, S_h(t_k)\right)}{h}\left(t - t_{k-1}\right) + \frac{\mathcal{F}_1\left(t_{k-1}, S_h(t_{k-1})\right)}{h}\left(t - t_k\right),\\
\mathcal{F}_2\left(s, E_h(s)\right) &\approx \frac{\mathcal{F}_2\left(t_k, E_h(t_k)\right)}{h}\left(t - t_{k-1}\right) + \frac{\mathcal{F}_2\left(t_{k-1}, E_h(t_{k-1})\right)}{h}\left(t - t_k\right),\\
\mathcal{F}_3\left(s, I_h(s)\right) &\approx \frac{\mathcal{F}_3\left(t_k, I_h(t_k)\right)}{h}\left(t - t_{k-1}\right) + \frac{\mathcal{F}_3\left(t_{k-1}, I_h(t_{k-1})\right)}{h}\left(t - t_k\right),\\
\mathcal{F}_4\left(s, B_v(s)\right) &\approx \frac{\mathcal{F}_4\left(t_k, B_v(t_k)\right)}{h}\left(t - t_{k-1}\right) + \frac{\mathcal{F}_4\left(t_{k-1}, B_v(t_{k-1})\right)}{h}\left(t - t_k\right),\\
\mathcal{F}_5\left(s, R_h(s)\right) &\approx \frac{\mathcal{F}_5\left(t_k, R_h(t_k)\right)}{h}\left(t - t_{k-1}\right) + \frac{\mathcal{F}_5\left(t_{k-1}, R_h(t_{k-1})\right)}{h}\left(t - t_k\right),
\end{aligned}
\tag{3.16}
$$

such that equation (3.15) yields

$$
\begin{aligned}
S_h(t_{m+1}) &= S_h(0) + \frac{(1-p)}{\mathcal{ABC}(p)}\mathcal{F}_1\left(t_m, S_h(t_m)\right) + \frac{p}{\mathcal{ABC}(p)\Gamma(p)}\sum_{k=0}^{m}\left(\frac{\mathcal{F}_1\left(t_k, S_h(t_k)\right)}{h}\mathcal{I}_{k-1,p}\right.\\
&\quad\left. + \frac{\mathcal{F}_1\left(t_{k-1}, S_h(t_{k-1})\right)}{h}\mathcal{I}_{k,p}\right),\\
E_h(t_{m+1}) &= E_h(0) + \frac{(1-p)}{\mathcal{ABC}(p)}\mathcal{F}_2\left(t_m, E_h(t_m)\right) + \frac{p}{\mathcal{ABC}(p)\Gamma(p)}\sum_{k=0}^{m}\left(\frac{\mathcal{F}_2\left(t_k, E_h(t_k)\right)}{h}\mathcal{I}_{k-1,p}\right.\\
&\quad\left. + \frac{\mathcal{F}_2\left(t_{k-1}, E_h(t_{k-1})\right)}{h}\mathcal{I}_{k,p}\right),\\
I_h(t_{m+1}) &= I_h(0) + \frac{(1-p)}{\mathcal{ABC}(p)}\mathcal{F}_3\left(t_m, I_h(t_m)\right) + \frac{p}{\mathcal{ABC}(p)\Gamma(p)}\sum_{k=0}^{m}\left(\frac{\mathcal{F}_3\left(t_k, I_h(t_k)\right)}{h}\mathcal{I}_{k-1,p}\right.\\
&\quad\left. + \frac{\mathcal{F}_3\left(t_{k-1}, I_h(t_{k-1})\right)}{h}\mathcal{I}_{k,p}\right),\\
B_v(t_{m+1}) &= B_v(0) + \frac{(1-p)}{\mathcal{ABC}(p)}\mathcal{F}_4\left(t_m, B_v(t_m)\right) + \frac{p}{\mathcal{ABC}(p)\Gamma(p)}\sum_{k=0}^{m}\left(\frac{\mathcal{F}_4\left(t_k, B_v(t_k)\right)}{h}\mathcal{I}_{k-1,p}\right.\\
&\quad\left. + \frac{\mathcal{F}_4\left(t_{k-1}, B_v(t_{k-1})\right)}{h}\mathcal{I}_{k,p}\right),\\
R_h(t_{m+1}) &= R_h(0) + \frac{(1-p)}{\mathcal{ABC}(p)}\mathcal{F}_5\left(t_m, R_h(t_m)\right) + \frac{p}{\mathcal{ABC}(p)\Gamma(p)}\sum_{k=0}^{m}\left(\frac{\mathcal{F}_5\left(t_k, R_h(t_k)\right)}{h}\mathcal{I}_{k-1,p}\right.\\
&\quad\left. + \frac{\mathcal{F}_5\left(t_{k-1}, R_h(t_{k-1})\right)}{h}\mathcal{I}_{k,p}\right),
\end{aligned}
\tag{3.17}
$$

where

$$
\begin{aligned}
\mathcal{I}_{k-1,p} &= \int_{t_k}^{t_{k+1}}\left(t - t_{k-1}\right)\left(t_{m+1} - t\right)^{\alpha-1}dt,\\
\mathcal{I}_{k,p} &= \int_{t_k}^{t_{k+1}}\left(t - t_k\right)\left(t_{m+1} - t\right)^{\alpha-1}dt.
\end{aligned}
$$

The above integrals $\mathcal{I}_{k-1,p}$ and $\mathcal{I}_{k,p}$ can be simplified as follows;

$$
\begin{aligned}
\mathcal{I}_{k-1,p} &= -\frac{1}{p}\left[(t_{k+1} - t_{k-1})(t_{m+1} - t_{k+1})^p - (t_k - t_{k-1})(t_{m+1} - t_k)^p\right] - \frac{1}{p(p-1)}\\
&\quad\times\left[(t_{m+1} - t_{k+1})^{p+1} - (t_{m+1} - t_k)^{p+1}\right],\\
\mathcal{I}_{k,p} &= -\frac{1}{p}\left[(t_{k+1} - t_{k-1})(t_{m+1} - t_{k+1})^p\right] - \frac{1}{p(p-1)}\left[(t_{m+1} - t_{k+1})^{p+1} - (t_{m+1} - t_k)^{p+1}\right].
\end{aligned}
\tag{3.18}
$$

By letting $t_k = kh$, equation (3.18) becomes

$$
\begin{aligned}
\mathcal{I}_{k-1,p} &= \frac{h^{p+1}}{p(p+1)}\left[(m+1-k)^p(m-k+2+p) - (m-k)^p(m-k+2+2p)\right],\\
\mathcal{I}_{k,p} &= \frac{h^{p+1}}{p(p+1)}\left[(m+1-k)^{p+1} - (m-k)^p(m-k+1+p)\right].
\end{aligned}
\tag{3.19}
$$

Substituting (3.19) into (3.17) gives the followings:

$$S_h(t_{m+1}) = S_h(0) + \frac{(1-p)}{\mathcal{ABC}(p)}\mathcal{F}_1(t_m, S_h(t_m)) + \frac{ph^p}{\mathcal{ABC}(p)\Gamma(p+2)}\sum_{k=0}^{m}\Big[\mathcal{F}_1(t_k, S_h(t_k)) \times \Big((m+1-k)^p(m-k+2+p) - (m-k)^p(m-k+2+2p)\Big) + \mathcal{F}_1(t_{k-1}, S_h(t_{k-1}))\Big((m+1-k)^{p+1} - (m-k)^p(m-k+1+p)\Big)\Big].$$

$$E_h(t_{m+1}) = E_h(0) + \frac{(1-p)}{\mathcal{ABC}(p)}\mathcal{F}_2(t_m, E_h(t_m)) + \frac{ph^p}{\mathcal{ABC}(p)\Gamma(p+2)}\sum_{k=0}^{m}\Big[\mathcal{F}_2(t_k, E_h(t_k)) \times \Big((m+1-k)^p(m-k+2+p) - (m-k)^p(m-k+2+2p)\Big) + \mathcal{F}_2(t_{k-1}, E_h(t_{k-1}))\Big((m+1-k)^{p+1} - (m-k)^p(m-k+1+p)\Big)\Big].$$

$$I_h(t_{m+1}) = I_h(0) + \frac{(1-p)}{\mathcal{ABC}(p)}\mathcal{F}_3(t_m, I_h(t_m)) + \frac{ph^p}{\mathcal{ABC}(p)\Gamma(p+2)}\sum_{k=0}^{m}\Big[\mathcal{F}_3(t_k, I_h(t_k)) \times \Big((m+1-k)^p(m-k+2+p) - (m-k)^p(m-k+2+2p)\Big) + \mathcal{F}_3(t_{k-1}, I_h(t_{k-1}))\Big((m+1-k)^{p+1} - (m-k)^p(m-k+1+p)\Big)\Big].$$

$$B_v(t_{m+1}) = B_v(0) + \frac{(1-p)}{\mathcal{ABC}(p)}\mathcal{F}_4(t_m, B_v(t_m)) + \frac{ph^p}{\mathcal{ABC}(p)\Gamma(p+2)}\sum_{k=0}^{m}\Big[\mathcal{F}_4(t_k, B_v(t_k)) \times \Big((m+1-k)^p(m-k+2+p) - (m-k)^p(m-k+2+2p)\Big) + \mathcal{F}_4(t_{k-1}, B_v(t_{k-1}))\Big((m+1-k)^{p+1} - (m-k)^p(m-k+1+p)\Big)\Big].$$

$$R_h(t_{m+1}) = R_h(0) + \frac{(1-p)}{\mathcal{ABC}(p)}\mathcal{F}_5(t_m, R_h(t_m)) + \frac{ph^p}{\mathcal{ABC}(p)\Gamma(p+2)}\sum_{k=0}^{m}\Big[\mathcal{F}_5(t_k, R_h(t_k)) \times \Big((m+1-k)^p(m-k+2+p) - (m-k)^p(m-k+2+2p)\Big) + \mathcal{F}_5(t_{k-1}, R_h(t_{k-1}))\Big((m+1-k)^{p+1} - (m-k)^p(m-k+1+p)\Big)\Big].$$

4. Numerical Simulation and Discussion

In this section, we present the simulation of the proposed numerical scheme from the previous section. For this purpose, we adopt the data in Table **??** along with the two sets

of positive initial values for the classes of fractional–order system (2.1)–(2.2) given in 2. The simulation of Data–I with different fractional orders $p \in (0,1)$ is shown in Figs. 2–6 while the simulation of Data–II with different fractional orders $p \in (0,1)$ is shown in Figs. 7–11.

Table 2: Values of Variables

Notation	**Data–I**	**Data–II**
$S_h(0)$	1270	6300
$E_h(0)$	300	820
$I_h(0)$	40	400
$B_v(0)$	20	200
$R_h(0)$	12	120

Table 3: Values of the parameters

Parameter	**Interpretation**	**Values**
Υ_h	Human shedding vibrose bacteria	0.047
ϕ	Half satuation Concentration vibrio cholerae	0.00027397
ν_h	Recruitment rate	0.024
μ_h	Natural death rate	$\frac{1}{65\times365}$
φ_h	Removal rate	0.098
ϖ	Motality rate caused by the disease	0.0279
ψ_h	Higher rate of virus transmission	0.00147
Θ_h	Rate of contact	0.25
ε	Progression rate	0.28

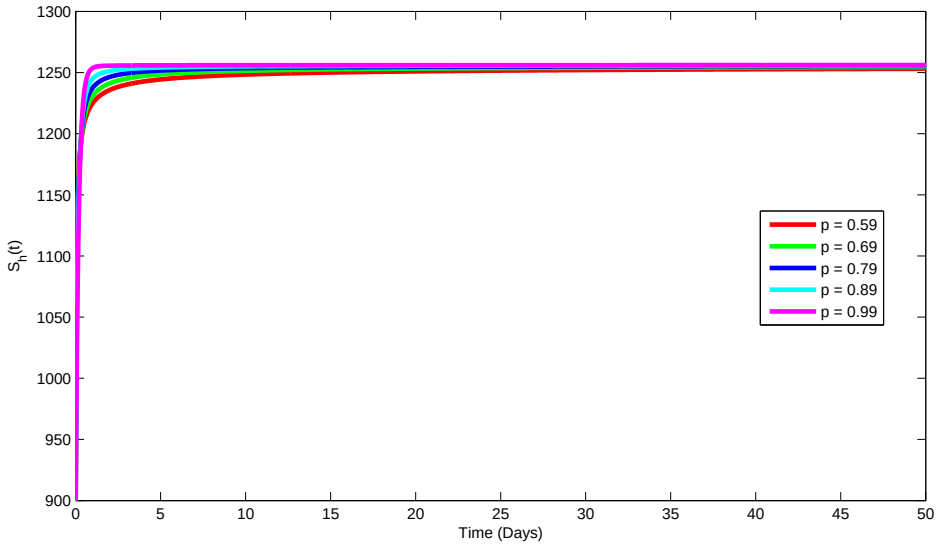

Figure 2: Dynamic of $S_h(t)$ at fractional orders between 0 and 1 and the initial values of Data–I.

.

Interpretation:
Figure 2 illustrates the dynamics of the susceptible human population, denoted by S_h, which shows a gradual increase over time before eventually stabilizing. Biologically, this rise in the susceptible compartment reflects the continuous influx of new individuals into the population through recruitment or birth, while disease-related deaths are assumed negligible (i.e., $\varpi = 0$). As a result, the pool of individuals at risk of infection continues to expand. Moreover, when the effective contact rate Θ_h among infected classes approaches zero—implying reduced transmission due to effective preventive measures such as vaccination, quarantine, social distancing, or reduced exposure—the probability of infection among susceptible individuals becomes minimal. Consequently, more individuals remain uninfected, leading to an accumulation in the susceptible class.

This biological behavior indicates that, in the absence of active transmission or mortality, the susceptible population will continue to grow and eventually stabilize at a steady state determined by the balance between recruitment and other natural demographic processes. However, if exposure resumes (i.e., if Θ_h increases), these susceptible individuals form a large pool that could drive a potential resurgence of infection.

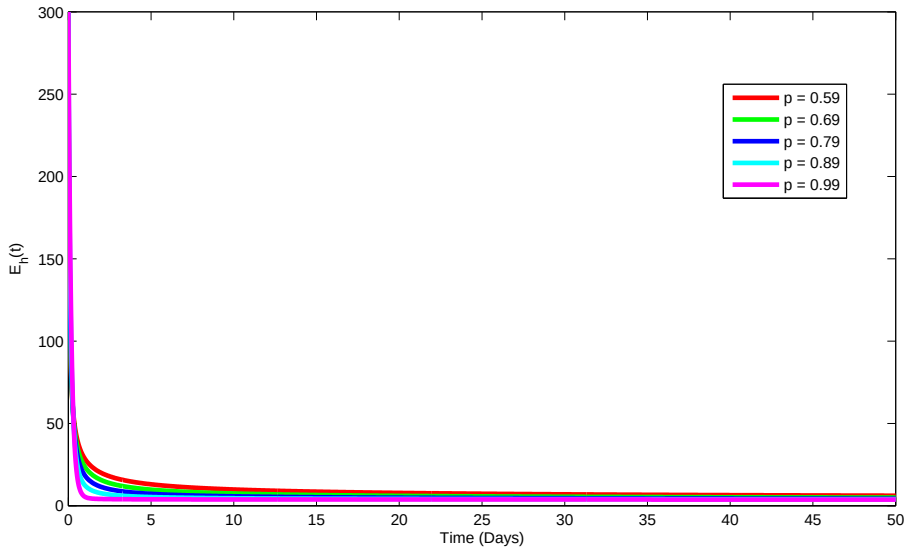

Figure 3: Dynamic of $E_h(t)$ at fractional orders between 0 and 1 and the initial values of Data–I.

.

Interpretation:
Figure 3 illustrates the dynamic behavior of the exposed human class, representing individuals who have been infected by the pathogen but are not yet infectious. The figure shows a rapid decline in the exposed population over a short period. Biologically, this decline reflects the quick progression of individuals from the latent (exposed) stage to the infectious stage, driven by the high transmission rate ψ_h of the disease within the population. A higher value of ψ_h indicates a faster rate at which exposed individuals become infectious, thereby shortening the incubation period and reducing the number of individuals remaining in the exposed class at any given time. This phenomenon signifies that once individuals are exposed, they rapidly progress to the infectious compartment, contributing to the spread of the disease.

Furthermore, this behavior highlights the biological implication that the exposed stage serves as a transitional phase whose duration is inversely related to the transmission intensity. Hence, controlling ψ_h through public health interventions—such as vaccination, early detection, or behavioral changes—can effectively slow down the rate at which exposed individuals develop into active cases, thereby reducing overall disease prevalence in the population.

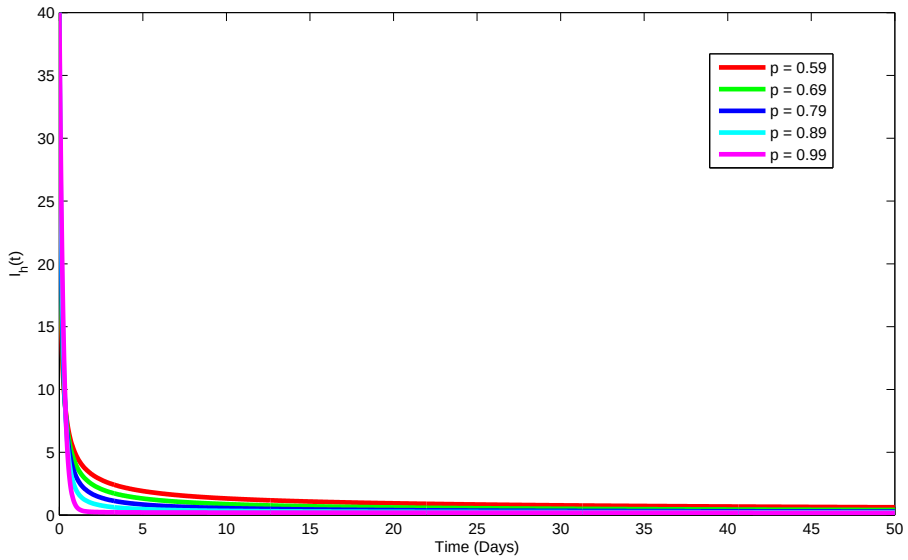

Figure 4: Dynamic of $I_h(t)$ at fractional orders between 0 and 1 and the initial values of Data–I.

.

Interpretation:
Figure 4 illustrates the dynamic behavior of the infected human class, which comprises individuals who are infectious and capable of transmitting the disease to others. The figure shows that this class experiences a decline in population over approximately 1 to 3 days, governed by the progression rate ε, as individuals from the exposed class transition into this category and later recover or are removed from the infectious pool. Biologically, this decline reflects the transient nature of infection in the population, where the rate of new infections and the rate of recovery or removal determine the overall size of the infected compartment. The observed pattern also underscores the role of the contact rate Θ_h, which regulates the flow of individuals from the susceptible class to the exposed class and subsequently into the infected class. An increase in Θ_h implies higher interaction between susceptible and infectious individuals, thereby elevating the risk of disease transmission. Consequently, more individuals become infected, leading to a reduction in the susceptible population. Conversely, a reduction in Θ_h—due to interventions such as social distancing, quarantine, vaccination, or improved hygiene—can slow down transmission, resulting in a smaller infected population over time.

This biological interpretation highlights the importance of controlling both the contact rate and the progression rate in managing disease spread, as these parameters jointly influence how quickly susceptible individuals become infectious and how rapidly the epidemic peaks and declines.

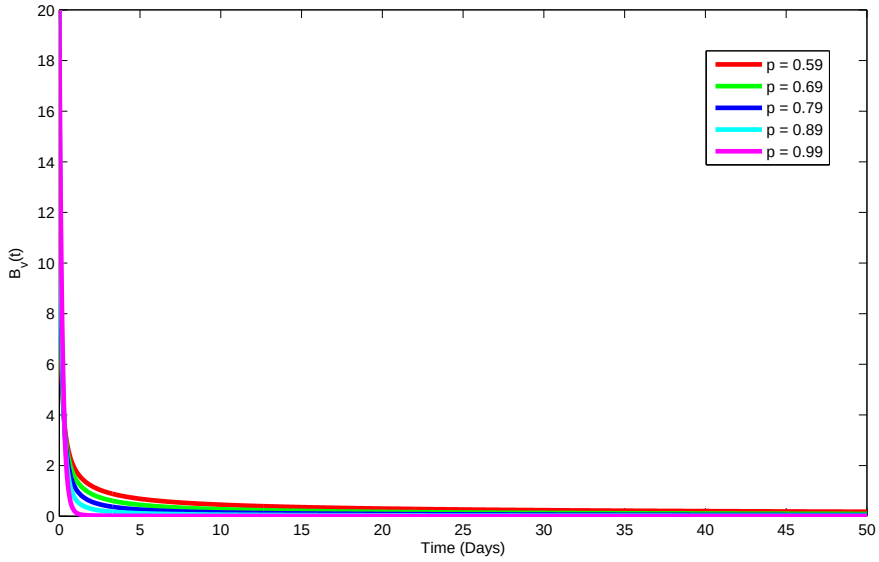

Figure 5: Dynamic of $B_\nu(t)$ at fractional orders between 0 and 1 and the initial values of Data–I.

.

The simualation depicts the concentration of vibro environment which shows decrease as time increases.

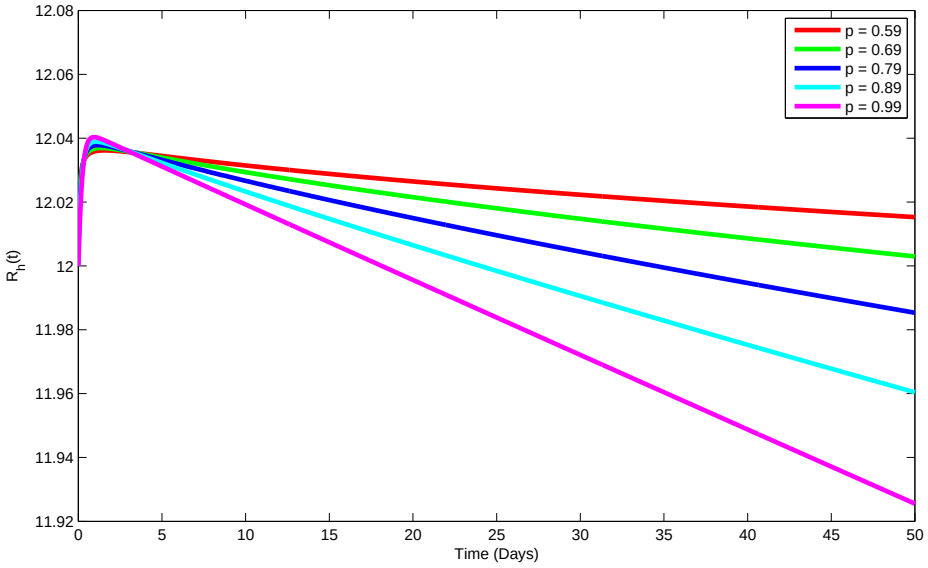

Figure 6: Dynamic of $R_h(t)$ at fractional orders between 0 and 1 and the initial values of Data–I.

.

Interpretation:
Figure 6 illustrates the dynamic behavior of the recovery or removed human class, which exhibits a rapid initial increase in population followed by a gradual stabilization over time. Biologically, this class represents individuals who have either recovered from infection after receiving effective treatment or have been removed from the population due to natural death (μ_h) or disease-induced death (ϖ). The observed rise in this compartment reflects the combined impact of treatment efficacy, natural recovery, and mortality associated with the disease. The simulation demonstrates that as more individuals transition from the infectious class—either through recovery or death—the size of the removed or recovered compartment increases correspondingly. This pattern underscores the importance of the removal rate, denoted by φ_h, which governs the outflow of individuals from the infectious class. A higher φ_h indicates an accelerated rate of recovery or removal, thereby reducing the infectious pool and contributing to disease control.

From a biological perspective, the stabilization of this class at later stages signifies that the epidemic is approaching equilibrium, where the number of new recoveries or deaths balances out with the depletion of infectious individuals. Hence, enhancing treatment rates and minimizing disease-induced deaths can significantly reduce infection persistence and promote long-term population stability.

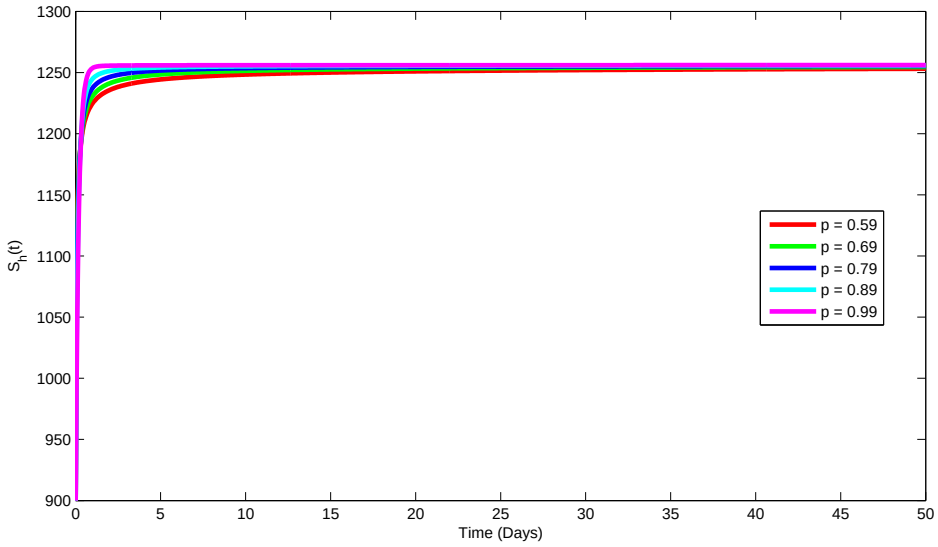

Figure 7: Dynamic of $S_h(t)$ at fractional orders between 0 and 1 and the initial values of Data–II.

.

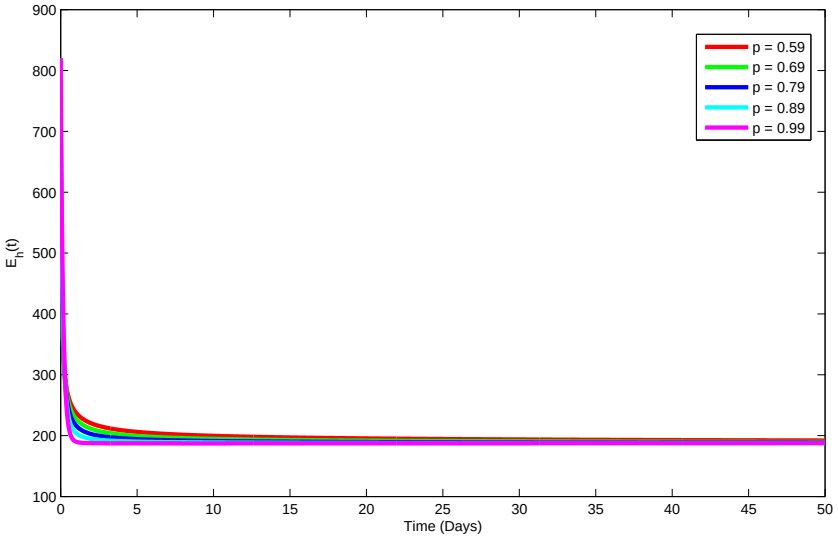

Figure 8: Dynamic of $E_h(t)$ at fractional orders between 0 and 1 and the initial values of Data–II.

.

Interpretation:
Figures 7–11 present the simulation results for the initial set of Data–II across all compartments of the fractional-order system described in equations (2.1)–(2.2). The overall simulation pattern appears almost identical to that of Data–I for the first four compart-

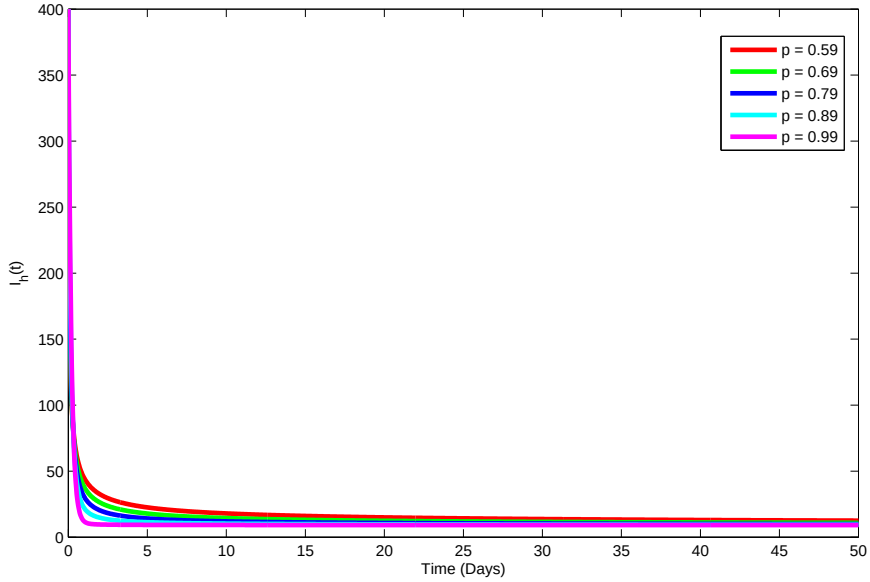

Figure 9: Dynamic of $I_h(t)$ at fractional orders between 0 and 1 and the initial values of Data–II.

.

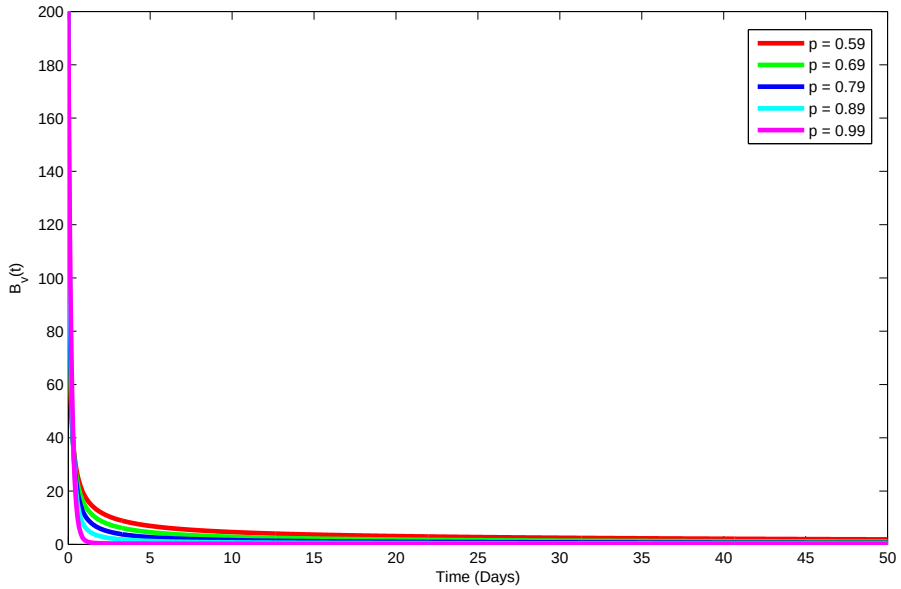

Figure 10: Dynamic of $B_v(t)$ at fractional orders between 0 and 1 and the initial values of Data–II.

.

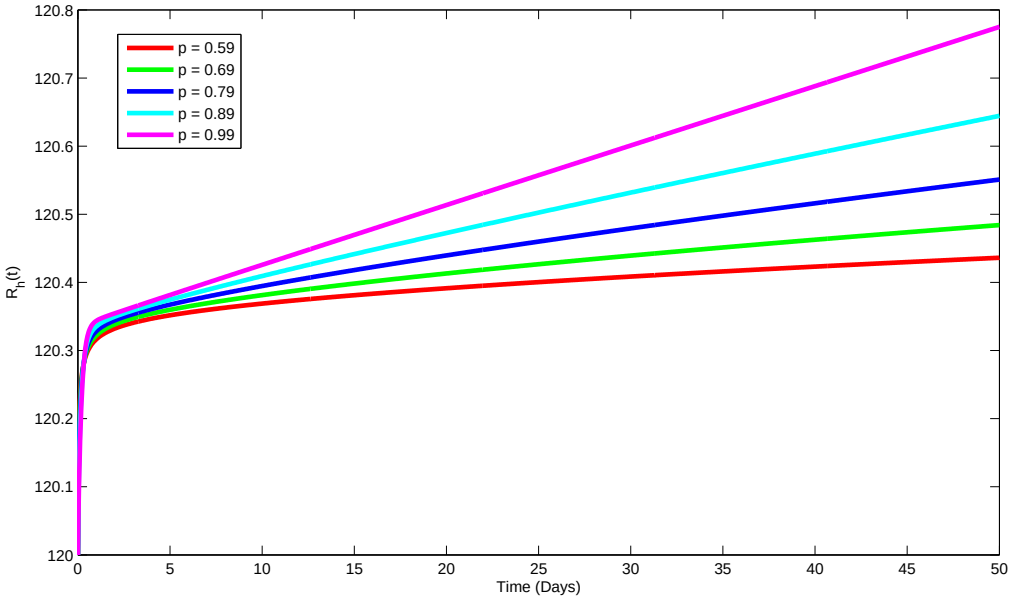

Figure 11: Dynamic of $R_h(t)$ at fractional orders between 0 and 1 and the initial values of Data–II.

.

ments, indicating consistent disease dynamics under both parameter sets. However, a notable difference is observed in the recovery or removed class, R_h, where the number of recovered individuals stabilizes more rapidly as time progresses.

Biologically, this rapid stabilization in the R_h compartment suggests an improved recovery process or effective disease management in the population represented by Data–II. This behavior may be attributed to factors such as enhanced treatment efficiency, improved public health interventions, or reduced reinfection and mortality rates. As a result, individuals recover more quickly and remain immune or removed from the transmission cycle, thereby diminishing the pool of infectious individuals.

Furthermore, the fractional-order framework captures the memory and hereditary effects inherent in disease transmission and recovery. The quicker stabilization of R_h implies that the system retains fewer long-term infection effects under the current parameter set, reflecting a more resilient population response. Hence, from a biological standpoint, the observed trend indicates that under the Data–II scenario, cholera recovery processes are more effective, leading to faster disease clearance and long-term epidemiological stability.

5. Conclusion

In this study, a fractional-order model for the transmission dynamics of cholera was developed and analyzed using the Atangana-Baleanu fractional derivative with a non-singular kernel. While traditional integer-order models have been commonly employed to describe infectious disease dynamics, the use of fractional-order derivatives has been shown to yield more realistic and precise results due to their non-local and non-singular

characteristics. These attributes allow the model to account for memory and hereditary effects, which are essential for understanding the long-term impact of past infections on disease progression.

The existence and uniqueness of the model's solution were rigorously established using Banach's and Krasnoselskii's fixed point theorems, and sufficient conditions to ensure these properties were identified. Analytical results indicated that the disease-free equilibrium is locally asymptotically stable when the basic reproduction number is less than one, suggesting that cholera can be effectively controlled under these circumstances.

Numerical simulations achieved through the predictor-corrector method in the Atangana-Baleanu sense corroborated the theoretical findings and provided further insights into the temporal dynamics of the various compartments. The susceptible population showed a gradual increase over time due to continuous recruitment and the absence of disease-related deaths, while the exposed class experienced a sharp decline as individuals moved to the infected stage, driven by the transmission rate. The infected class initially grew and then decreased as individuals either recovered or succumbed to the disease. In contrast, the recovered (or removed) class exhibited a rapid rise before stabilizing, reflecting treatment effects and natural mortality.

Overall, the findings indicate that the incorporation of fractional-order derivatives considerably improves the realism and adaptability of epidemic models. The fractional parameter has a significant impact on the dynamics of the disease, providing a more thorough understanding of cholera transmission and management strategies. This study highlights the value of fractional-order modeling as an effective tool for predicting, analyzing, and controlling the spread of infectious diseases like cholera.

5.1. Recommendations and Future Work

Based on the findings of this study, several recommendations and directions for future research are proposed to enhance understanding and control of cholera transmission dynamics:

1. **Public Health Interventions:** The results indicate that effective control of cholera can be achieved when the basic reproduction number remains below one. Therefore, it is recommended that public health agencies intensify efforts in *environmental sanitation*, *safe water supply*, and *public health education* to reduce the transmission rate and minimize exposure to contaminated sources.
2. **Model Parameter Refinement:** Future studies should incorporate *real epidemiological data* from different regions to estimate model parameters more accurately. This will help validate the fractional–order model and improve its predictive performance under varying environmental and demographic conditions.
3. **Inclusion of Control Strategies:** The present study did not explicitly consider intervention measures such as *vaccination*, *treatment optimization*, or *public health campaigns*. Extending the model to include these control strategies within a fractional–order framework will provide deeper insights into the combined effects of multiple interventions on disease eradication.
4. **Comparative Analysis:** A comparative study between *integer–order* and *fractional–order* cholera models is recommended to quantify the extent of improvement in

accuracy and realism contributed by the fractional derivative, especially in long–term disease prediction.

5. **Extension to Multi–Host and Spatial Models:** Future work may also extend this model to incorporate *spatial heterogeneity*, *multiple host populations*, or *environmental reservoirs*, allowing the investigation of spatial–temporal patterns of cholera outbreaks.
6. **Exploration of Alternative Fractional Operators:** Other *non–local fractional derivatives* such as the *Caputo–Fabrizio* and *Prabhakar* derivatives could be employed for comparison to assess how different memory kernels influence the transmission dynamics and solution behavior.

In conclusion, this study establishes a strong foundation for exploring fractional–order epidemic modeling as a more realistic and flexible framework. Future research incorporating additional control mechanisms, real data, and extended system structures will further improve the understanding and management of cholera and similar infectious diseases.

References

[1] Aatif A., Saeed I., Khan M.R., Rasheed S., Allehiany F.M., Baili J., Muhammad A. K., Hijaz A., (2021) Dynamics of a fractional order Zika virus model with mutant, Alex. Eng. Journ.

[2] Abbas, M., Kumar, S., & Alshomrani, A. S. (2024). Study of chronic myeloid leukemia with T-cell under fractal-fractional order model. Open Physics, 22(1), 20240032. https://doi.org/10.1515/phys-2024-0032

[3] Abbas, M., Kumar, S.,& Alshomrani, A. S. (2024). Statistical and computational analysis for corruption and poverty model using Caputo-type fractional differential equations. Heliyon, 10(3), e24424. https://doi.org/10.1016/j.heliyon.2024.e24424

[4] Abbas, M., Kumar, S., & Alshomrani, A. S. (2024). Analysis of nonlinear Burgers equation with time fractional Atangana–Baleanu–Caputo derivative. Heliyon, 10(13), e26102. https://doi.org/10.1016/j.heliyon.2024.e26102

[5] Andrew, J.R and Basu, (2011) Trasmission dynamics and control of cholera in Haiti: an epidemic model cancel,377(9773),1248-1255..

[6] Atangana A. and Araz S.I.,(2020) Mathatical model of COVID-19 spread in Turkey and South Africa: theory, methods and applications, Advances in Diff. Eqns,2020:659,

[7] Atangana A. and Araz S.I., (2021) A novel Covid-19 model with fractional differential operators with singular and non-singular kernels: Analysis and numerical scheme based on Newton polynomial, Alexandria Eng Jour. 2021, http://doi.org/10.1016/j.aej.2021.02.016.

[8] Atangana A. and Seda I.A.,(2021) Modeling third waves of Covid-19 spread with piecewise differential and integral operators: Turkey, Spain and Czechia, Results in Physics 29 104694.

[9] Baleanu D.,Jajarmi A.,Mohammadi H., and RezapourS.,(2020) A new study on the mathematical modelling of human liver with Caputo-Fabrizio fractional derivative. Chaos Solitons Fractals 134, 109705.

[10] Burton T.A.,(1998). A fixed point theorem of Krasnoselskii, Appl. Math. Lett., Vol 11, Issue 1.

[11] Chima,(2022). Mathematical models of control measures in the spread of cholera, maths and statistics,

[12] Deressa, C.T., and Duressa, G.F.,(2021). Modeling and optimal control analysis of transmission dynamics of COVID-19: the case of Ethiopia. Alex. Eng. J. 60(1), 719-732.

[13] Driessche, V.D. and Watmough J.,(2002) Reproduction numbers and sub-threshold endemic equilibria for compartmental models of disease transmission, Math. Biosci. 180(1), 29-48.

[14] Farai, N., Jennifer M. A., and Josiah M.,(2019) Modelling cholera transmission dynamics in the presence of limited resources, https://doi.org/10.1186/5/3104-019-4504-9

[15] Faruque, S. M., Albert, M. J., and Mekalanos, J.J, (1961) Epidemiology, genetics, and ecology of toxigenic vibrio cholerae. Microbiology and Molecular Biology Reviews, 62(4), 1301–1314.

[16] Finkelstein, R. A. (1996). Medical microbiology, 4th edition. University of Texas Medical Branch at Galveston.

[17] Helikumi M.,Kgosimore M., Kuznetsov D.and Mushayabasa S.,(2020) Dynamical and optimal control analysis of a seasonal Trypanosoma brucei rhodesiense model, Math. Biosci. Eng.17, 2530?2556. https://doi.org/10.3934/mbe.2020139.

[18] Helikumi M.,(2022) A note on fractional-order model for cholera disease transmission with control strategies.ISSN 2052-2541

[19] Jan R., Khan M.A., Kumam P., Thounthong P., (2019)Modeling the transmission of dengue infection through fractional derivatives, Chaos Solit. Fract. 127 189-216.

[20] Iwa L.L, Nwajeri U.K., Attede A.O., Panle A.B., Egeonu K.U.,(2023) Malaria and cholera co–dynamics model analysis furnished with fractional–order differential equations, Math. Modelling and Numer. Appl.

[21] Khan M.A and Atagana A.,(2020) *Modelling the dynamics of novel coronavirus (2019-nCOV) with fractional derivative*, Alexandria Eng. J., https://doi.org/10.1016/j.aej.2020.02.033.

[22] Lina Q., Zhaob S., Gaod D., Loue Y., Yang S., Salihu S. M., Wang M.H., Caig Y., Weiming W.,Yangh L., Daihai H.,(2020) A conceptual model for the Coronavirus disease 2019 (COVID-19) outbreak in Wuhan, China with individual reaction and governmental action, Int. Jour. of Infectious Diseases 93 211-216.

[23] Mariam, C., and Ronald W.,(2016) Cholera pathology. Available from http://www.britannica.com/science/cholera(Accessed:20-April)

[24] Mintz, E. D., and Tauxe, R. V.,(2013) Cholera in Africa: A closer look and a time for action. Journal of Infectious Diseases, 208(suppl 1), S4–S7.

[25] Mari, L., Berthuzzo E., Righetto L., CasagrandiR., Gatti M., and Rodriquezi I.,(2011) Modelling cholera epidemics: the role of water ways, human mobility and sanitation. Journal of the Royal Society interface. https://doi.org/10.1016/j.chaos.2020.109705.
[26] Mohammadi H.,Kumar S, Rezapour S.,Etemad S.,(2021) A theoretical study of the Caputo-Fabrizio fractional modeling for hearing loss due to Mumps virus with optimal control. Chaos Solitons Fractals 144, 110668.https://doi.org/10.1016/j.chaos.2021.110668.
[27] Nelson, E.J., Harris, J.B., Morris, J.G., Calderwood, S.B., Camilli, A,(2009). Cholera transmission: the host, pathogen and bacteriophage dynamics, Nat. Rev. Microbiol 7 693702.
[28] Nwajeri U.K., A. Omame, C.P. Onyenegecha,(2021) Analysis of a fractional order model for HPV and CT co-infection, Results in Physics.
[29] Nwajeri U.K, Panle A.B, Omame A, Obi M.C, Onyenegecha C.P.,(2022) On the fractional order model for HPV and Syphilis using non-singular kernel, Results in Physics;37:105463.
[30] Ndolane S.,(2021) Fractional advection-dispersion equation described by the Caputo left generalized fractional derivative, Palestine Journal of Mathematics, Vol. 10(2), 562-579. https://doi.org/10.1016/j.rinp.2022.105463.
[31] Owolabi K.M. and Atangana A.,(2019) Numerical Methods for Fractional Differentiation, Springer Nature Singapore Pte Ltd.
[32] Oldham K.B.and Spanier J.,(1974) The fractional calculus, mathematics in sc. and eng., Vol. 111. Academic Press.
[33] Ogunrinde R.B., Nwajeri U.K., Fadugba S.E., Ogunrinde R.R., Oshinubi K.I.,(2021) Dynamic model of COVID-19 and citizens reaction using fractional derivative. Alexandria Eng Journ. ;60(2):2001-12.
[34] Okolo P.N., Magaji A.S, Isaac J and Usemi P.F.,(2020) Mathematical modelling and analysis of cholera disease dynamics with control, http://doi.org/10.33003/fjs-2020-0404-494.
[35] Ogunrinde R.B, Nwajeri U.K, Fadugba S.E, Ogunrinde R.R. and Oshinubi K.I. *Dynamic model of COVID-19 and citizens reaction using fractional derivative*, Alexandria Eng. Jour., Vol. 60, Issue 2, Pages 2001-2012.(2021).
[36] Omame A., Abbas, M., Nwajeri UK.,(2022) A fractional-order control model for Diabetes COVID-19 co-dynamics with Mittag-Leffler function, Alexandria Eng J, https://doi.org/10.1016/j.aej.2022.01.012.
[37] Omame A., Okuonghae D., Nwajeri U.K. and Onyenegecha C.P.,(2022) A fractional-order multi-vaccination model for COVID-19 with non-singular kernel, Alex. Eng. Jour., Vol. 61, Issue 8, 6089-6104.
[38] Owolabi K.M. and Atangana A.,(2019), Numerical Methods for fractional differentiation, Springer series in Comp. Math., 2019.
[39] Pollitzer, R, (1954) Cholera studies. 1. History of the disease. Bulletin of the World Health Organization, 10(3), 421, .
[40] Podlubny I.,(1999) Fractional differential equations: an introduction to fractional derivatives, fractional differential equations, to methods of their solution and some of their applications, Academic Press, San Diego.
[41] Rezapour S., Mohammadi H., Jajarmi A.,(2020) A new mathematical model for Zika virus transmission. Adv. Differ. Equ. 2020, 589 . https://doi.org/10.1186/s13662-020-03044-7.
[42] Shah S.A.A., Khan M.A., Farooq M.,Ullah E.O. and Alzahran A.,(2020) fractional order model for Hepatitis B virus with treatment via Atangana?Baleanu derivative, Physica A: Stat. Mech. Appl. 538 , 122636. https://doi.org/10.1016/j.physa.2019.122636.
[43] Skanchy, H., Chantry, J., and Nielsen, S.(2009) An epidemiological look at cholera. Available from http://www.citeseerx.ist.psu.edu/
[44] Toufik M., and Atangana A.,(2017) New numerical approximation of fractional derivative with non-local and non–singular kernel: Application to chaotic models, Eur. Phys. J. Plus 132(10) (2017) 444.
[45] WHO Cholera fact sheet number 107: December, 2017a, http://www.who.int/mediacentre/factsheets/fs107/en/.
[46] World Health Organization. (2010). Cholera vaccines: Who position paper. Available from http://www.who.int/wer/2010/wer8513.pdf.uad, 11-July-2016
[47] Yang, C., & Chayu, Y. (2020). Mathematical modelling, analysis, and simulation of cholera dynamics. Journal Name, Volume(Issue), pages. DOI